

See discussions, stats, and author profiles for this publication at: <https://www.researchgate.net/publication/41415371>

Studying the Origin of the Antiferromagnetic to Spin-Canting Transition in the β -p-NCC6F4CNSSN. Molecular Magnet

ARTICLE in CHEMISTRY - A EUROPEAN JOURNAL · FEBRUARY 2010

Impact Factor: 5.73 · DOI: 10.1002/chem.200903221 · Source: PubMed

CITATIONS

25

READS

58

7 AUTHORS, INCLUDING:



Mercè Deumal

University of Barcelona

56 PUBLICATIONS 818 CITATIONS

SEE PROFILE



Jeremy M Rawson

University of Windsor

241 PUBLICATIONS 3,302 CITATIONS

SEE PROFILE



Michael A Robb

Imperial College London

351 PUBLICATIONS 16,256 CITATIONS

SEE PROFILE



Juan J. Novoa

University of Barcelona

276 PUBLICATIONS 5,500 CITATIONS

SEE PROFILE

Studying the Origin of the Antiferromagnetic to Spin-Canting Transition in the β -*p*-NCC₆F₄CN₂SSN⁺ Molecular Magnet

Mercè Deumal,^{*,[a]} Jeremy M. Rawson,^[b] Andrés E. Goeta,^[c] Judith A. K. Howard,^[c] Royston C. B. Copley,^[c] Michael A. Robb,^[d] and Juan J. Novoa^{*,[a]}

Abstract: The crystal structure of the spin-canted antiferromagnet β -*p*-NCC₆F₄CN₂SSN⁺ at 12 K (reported in this work) was found to adopt the same orthorhombic space group as that previously determined at 160 K. The change in the magnetic properties of these two crystal structures has been rigorously studied by applying a first-principles *bottom-up* procedure above and below the magnetic transition temperature (36 K). Calculations of the magnetic exchange pathways on the 160 K structure reveal only one significant exchange coupling ($J(d1) = -33.8 \text{ cm}^{-1}$), which generates a three-dimensional diamond-like magnetic topology within the crystal. The com-

puted magnetic susceptibility, $\chi(T)$, which was determined by using this magnetic topology, quantitatively reproduces the experimental features observed above 36 K. Owing to the anisotropic contraction of the crystal lattice, both the geometry of the intermolecular contacts at 12 K and the microscopic J_{AB} radical–radical magnetic interactions change: the $J(d1)$ radical–radical interaction becomes even more antiferromagnetic (-43.2 cm^{-1}) and two additional ferromagnetic interactions

appear ($+7.6$ and $+7.3 \text{ cm}^{-1}$). Consequently, the magnetic topologies of the 12 and 160 K structures differ: the 12 K magnetic topology exhibits two ferromagnetic sublattices that are antiferromagnetically coupled. The $\chi(T)$ curve, computed below 36 K at the limit of zero magnetic field by using the 12 K magnetic topology, reproduces the shape of the residual magnetic susceptibility (having subtracted the contribution to the magnetization arising from spin canting). The evolution of these two ferromagnetic J_{AB} contributions explains the change in the slope of the residual magnetic susceptibility in the low-temperature region.

Keywords: ab initio calculations • diazo radicals • magnetic properties • spin canting • X-ray diffraction

Introduction

In 1928, Heisenberg proposed that bulk magnetic order would only be achieved in systems containing atoms for which the principal quantum number is greater than two, inferring transition-metal and lanthanide ions (i.e., in systems in which the unpaired electron(s) are located on metal ions), although this does not necessarily exclude heavy p-block elements.^[1] However, in 1991, Kinoshita and co-workers reported the discovery of bulk ferromagnetism in a purely organic radical, the β polymorph of the *p*-nitrophenyl nitronyl nitroxide, *p*-NPNN ($T_C = 0.6 \text{ K}$).^[2] Since then, a large number of organic radicals have been shown to undergo bulk magnetic order, although the majority do so below 1 K.^[3] A small number of C/N/O-based radicals order above 1 K, including the radical [C₆₀][TDAE] cation salt ($T_C = 16 \text{ K}$; TDAE = tetrakis(dimethylamino)ethylene),^[4] the DOTMDAA neutral radical ($T_C = 1.48 \text{ K}$; DOTMDAA = *N,N'*-dioxy-1,3,5,7-tetramethyl-2,6-diazaadamantane),^[5] and an oxo-verdazyl radical ($T_N = 5.4 \text{ K}$).^[6]

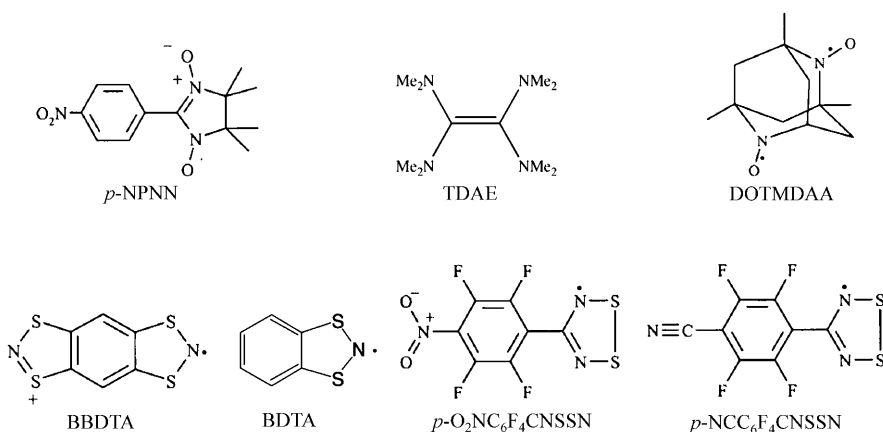
[a] Dr. M. Deumal, Prof. J. J. Novoa
Departament de Química Física & IQTCUB
Universitat de Barcelona, Martí i Franquès 1
08028, Barcelona (Spain)
Fax: (+34) 93-402-1231
E-mail: merce.deumal@ub.edu
juan.novoa@ub.edu

[b] Dr. J. M. Rawson
Department of Chemistry, the University of Cambridge
Lensfield Road, Cambridge CB2 1EW (UK)

[c] Dr. A. E. Goeta, Prof. J. A. K. Howard, Dr. R. C. B. Copley
Department of Chemistry, Durham University
South Road, Durham DH1 3 LE (UK)

[d] Prof. M. A. Robb
Department of Chemistry, Imperial College London
South Kensington Campus, London SW7 2AZ (UK)

Supporting information for this article is available on the WWW under <http://dx.doi.org/10.1002/chem.200903221>.



Recent studies indicate that free radicals based upon heavier p-block elements such as S and Se offer higher ordering temperatures.^[7] In the family of dithiazolyl radicals [BBDTA][GaCl₄] (BBDTA = benzo(bis-1,3,2-dithiazolyl)) orders as a ferromagnet below $T_C = 6.7$ K,^[8] whereas BDTA (BDTA = benzo-1,3,2-dithiazolyl) exhibits antiferromagnet-

Abstract in Catalan: L'estructura cristal·lina de l'antiferromagnet amb spin-canting β -p-NCC₆F₄CNSSN ha estat caracteritzada a 160 K i a 12 K (aquest treball), determinant-se que pertanyen al mateix grup espacial ortoròmbic Fdd2. Entorn de la temperatura de transició magnètica (36 K), el canvi en les propietats magnètiques d'aquests dos cristalls és estudiat amb rigorositat aplicant un procediment de treball bottom-up basat en primers principis. El càlcul de camins de bescanvi magnètic usant l'estructura de 160 K revela només un acoblament magnètic significatiu ($J(dI) = -33.8$ cm⁻¹), que genera una topologia magnètica tridimensional de tipus diamant dins del cristall. La susceptibilitat magnètica $\chi(T)$ calculada usant aquesta topologia magnètica reproduïx quantitativament els trets experimentals observats per sobre de 36 K. A causa de la contracció anisotròpica de la xarxa cristal·lina, a 12 K hi ha canvis tant en la geometria dels contactes intermoleculars com en la magnitud de les interaccions magnètiques microscòpiques entre radicals, J_{AB} : $J(dI)$ es torna encara més antiferromagnètica (-43.2 cm⁻¹) i apareixen dues interaccions ferromagnètiques addicionals ($+7.6$ i $+7.3$ cm⁻¹). Les topologies magnètiques de les estructures a 12 K i a 160 K són doncs diferents: la topologia magnètica a 12 K presenta dues sub-xarxes ferromagnètiques acoblades antiferromagnèticament. La corba $\chi(T)$ calculada per sota de 36 K en el límit de camp magnètic zero usant la topologia magnètica a 12 K reproduïx la forma de la susceptibilitat magnètica residual (un cop la contribució a la magnetització provinent de l'spin-canting ha estat restada). L'evolució de les dues contribucions ferromagnètiques J_{AB} explica el canvi en el pendent de la susceptibilitat magnètica residual a la regió de baixa temperatura.

ism below 11 K when rapidly cooled.^[9] A selenathiazolyl has recently been reported to order as a ferromagnet below $T_C = 12.3$ K,^[10a] and its isoelectronic analogues generated by substitution of S for Se have been shown to order at $T_C = 17$ K.^[10b] A series of thia or selenazyl derivatives have also been shown either to order as weak (spin-canted) ferromagnets with $T_C = 18$ K and 27 K,^[11a] or to present marked differences in conductivity, which can be enhanced by applying physical pressure.^[11b] These studies underline

the effect that inclusion of heavier heteroatoms enhances not only charge transport, but also magnetic exchange interactions.

In the family of dithiadiazolyl radicals, p -O₂NC₆F₄CNSSN[•] orders as a ferromagnet ($T_C = 1.3$ K)^[12] whereas the β phase of p -NCC₆F₄CNSSN[•] exhibits canted antiferromagnetism below 36 K.^[13–16] Previous theoretical studies of the magnetism of β -p-NCC₆F₄CNSSN[•],^[17] based on a crystal structure at 160 K, revealed a single dominant magnetic exchange pathway in the high-temperature regime. The objective of this paper is to gain a better, and theoretically sound, understanding of the paramagnetic and canted antiferromagnetic (also known as weak ferromagnetic) regions, as well as the origin of the magnetic transition at 36 K in the β -p-NCC₆F₄CNSSN[•] magnet. With this aim, we apply a first-principles *bottom-up* procedure to study its magnetic properties by using structural data collected above (160 K)^[13a–16] and below (12 K, reported in this work) the magnetic transition temperature (36 K). We show that there is a significant temperature dependence of the magnetic exchange interactions associated with the asymmetric contraction of the unit cell, with the evolution of additional microscopic pair-wise J_{AB} magnetic exchange terms upon cooling. This leads to a more complex magnetic topology in the low-temperature region with three non-negligible J_{AB} interactions at 12 K: one strong antiferromagnetic interaction and two weaker ferromagnetic interactions. The first-principles *bottom-up* procedure that was carried out by using the 160 K crystal structure shows that the magnetic response in the paramagnetic region can be quantitatively modeled with a single exchange term based on a 3D diamond-like network. Conversely, the 12 K magnetic topology can be described as two strongly antiferromagnetically coupled ferromagnetic sublattices, that is, as a competition between two ferromagnetic sublattices of similar shape and strength coupled antiferromagnetically, a fact that can justify the presence of canting below 36 K. The magnetic susceptibility curve computed from the low-temperature magnetic topology reproduces the magnetic response in the low-temperature region once the contribution arising from spin canting has been subtracted.

In the β - p -NCC₆F₄CN₂SSN* magnet, the transition temperature rises from 36 K at ambient pressure to in excess of 65 K under 16 kbar pressure.^[18] The magnetic exchange interactions in the crystal structure of β - p -NCC₆F₄CN₂SSN* are strong, as evidenced by a large Weiss constant ($\theta = -102$ K) for the Curie–Weiss fit of the high-temperature region.^[13] The mean-field approach^[19] to the Curie–Weiss law allows a first estimate of the strength of the exchange coupling from the relationship given in [Eq. (1)]:

$$\theta = 2zJS(S+1)/3k \quad (1)$$

in which z is the number of nearest-neighbor interactions ($z=4$ according to the S...N contacts found in β - p -NCC₆F₄CN₂SSN* crystal at 160 K), yielding $J/k = -34$ cm⁻¹. The magnetic susceptibility $\chi(T)$ passes through a broad maximum around 60 K, indicative of short-range antiferromagnetic spin correlations, prior to ordering as a canted antiferromagnet below 36 K.^[13] The in-phase component χ' of the ac susceptibility studies^[14] shows a peak at 36 K, which precedes the onset of bulk magnetic order. The thermal evolution of the out-of-phase component χ'' is considerably more complex because it is not detected until approximately 28 K (i.e., 8 K below T_C), and then rapidly rises upon cooling to 20 K where it reaches a plateau before increasing again below 12 K. Single-crystal EPR,^[20] dc susceptibility,^[13a] and powder μ -SR (muon spin relaxation) studies^[15] all reveal the onset of a spontaneous magnetic moment below 36 K and also that the saturation of the magnetization below the transition temperature follows the Brillouin function. Finally, low-temperature EPR,^[20] powder neutron,^[14] and μ -SR^[15] studies have indicated that the experimental magnetic structure has the b axis as the easy axis of alignment. No evidence for a structural phase transition at 36 K has been identified in any of these studies.^[13a–16, 18, 20]

A number of theoretical models have been put forward to rationalize both the sign and the magnitude of intra- and intermolecular magnetic exchange in organic systems.^[21, 22] Amongst the most popular mechanisms for rationalizing intermolecular exchange is the so-called McConnell-I mechanism, the common use of which is based upon the overlap of regions of positive and negative spin density.^[23, 24] Although this works in a number of cases, a survey of a large group of nitronyl nitroxide derivatives showed that there was no apparent correlation between intermolecular N...O distances or angles and the sign of J_{AB} between radicals, which goes against what was to be predicted by the McConnell-I mechanism.^[25] However, nowadays it is possible to make an accurate quantitative evaluation of not only the sign and magnitude of the magnetic interactions, but also to predict the macroscopic magnetic properties of molecule-based magnets by performing a first-principles *bottom-up* study of the crystal.^[26] The good performance of this procedure has been demonstrated in a variety of crystals.^[27–32]

Experimental Section

A sample of p -NCC₆F₄CN₂SSN* was prepared according to the literature method^[13a] and crystals of the β phase formed as long needles by sublimation in a static vacuum (10^{-1} Torr, 90–40 °C).

X-ray crystallography: Single-crystal X-ray diffraction data were collected at 12 K on the Fddd diffractometer^[33] equipped with a Displex cryo-refrigerator. Data were obtained up to 60° in 2θ by using graphite monochromated Mo_{K α} radiation ($\lambda = 0.71073$ Å) from a needle-shaped black single crystal ($0.02 \times 0.02 \times 0.10$ mm). The crystal was mounted on a sharpened 0.3 mm graphite propelling pencil lead (by using low-temperature Oxford Instruments TRZ0004 epoxy glue) to enhance thermal conduction when using the Displex cryo-refrigerator, because cooling of the sample was achieved through the fiber and the mount. The Fddd diffractometer was controlled by the MAD software^[34] and reduction of data from this instrument was performed by using the COLL5N program.^[35] The structure was solved by using direct methods^[36] and was refined^[37] by using full-matrix least squares methods on F^2 . Table 1 shows the crystal and refinement data for the 12 K dataset.

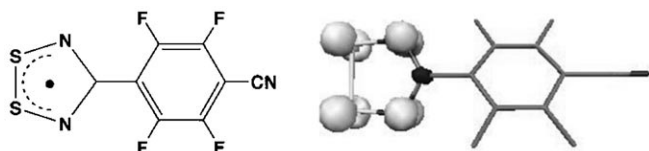
CCDC-755508 contains the supplementary crystallographic data for this paper. These data can be obtained free of charge from The Cambridge Crystallographic Data Centre via www.ccdc.cam.ac.uk/data_request/cif.

Table 1. Crystallographic data for β - p -NCC₆F₄CN₂SSN* at 12 K (CCDC-755508).

Formula	C ₈ F ₄ N ₃ S ₂
M_r	278.23
crystal system	orthorhombic
space group	<i>Fdd2</i>
T [K]	12
a [Å]	14.913(3)
b [Å]	10.735(2)
c [Å]	11.925(2)
V [Å ³]	1909.1(7)
Z	8
ρ_{calcd} [mg m ⁻³]	1.936
μ (Mo _{Kα}) [mm ⁻¹]	0.595
measured reflns	5700
independent reflns	1393
$[I > 2\sigma(I)]$ reflns	1327
R_{int}	0.0463
θ_{max} [°]	60.00
$R[F^2 > 2\sigma(F^2)]$	0.0291
$wR(F^2)$	0.0724
S	1.08
refined parameters	81
$(\Delta/\sigma)_{\text{max}}$	0.004
$\Delta\rho_{\text{max}}, \Delta\rho_{\text{min}}$ [e Å ⁻³]	0.513, -0.338

Computational details: The first-principles *bottom-up* theoretical procedure^[26] computes the bulk magnetic properties of a compound by using just the crystallographic data. This first-principles *bottom-up* approach requires four steps:

Step 1) Analysis of the crystal structure to identify all unique radical–radical pairs present in the crystal: The magnetic interactions between p -NCC₆F₄CN₂SSN* radicals in the 12 and 160 K crystals are through space (also called direct exchange magnetic interactions). Each p -NCC₆F₄CN₂SSN* unit is a doublet radical (see Scheme 1). Calculations of the spin-density distribution in the p -NCC₆F₄CN₂SSN* radical from both frozen-solution EPR spectra and DFT calculations are in excellent agreement,^[14, 16] and indicate that the spin density is delocalized over the heterocyclic S and N atoms with a small negative spin density at the heterocyclic C atom and very small positive spin density on the two *ortho*-F atoms of the perfluorophenyl substituent (see Scheme 1). Recent polarized single-crystal neutron diffraction experiments on the closely related p -



Scheme 1.

$\text{O}_2\text{NCC}_6\text{F}_4\text{CNSSN}^\bullet$ radical confirm this spin distribution.^[38] Because the spin density is mainly delocalized on the dithiadiazolyl ring (see Scheme 1), the criterion to select radical–radical pairs was based upon heterocyclic $\text{NSSNC}\cdots\text{CNSSN}$ distances smaller than 13.00 Å. This cut-off point includes all nearest-neighbor and closest next-nearest-neighbor contacts.

Step 2) Computation of the microscopic magnetic interactions (J_{AB}) for each unique radical–radical pair AB found in the crystal: For through-space interactions, the microscopic exchange pair-wise coupling J_{AB} appears to be local and there is no need to account for cooperative effects by using larger clusters. Indeed, the magnetic exchange values J_{AB} extracted from tri- and tetraradical models were practically the same as for the dimer model. This dimer approach has been previously shown to perform adequately for a variety of through-space magnetic molecular systems.^[39] Because the $p\text{-NCC}_6\text{F}_4\text{CNSSN}^\bullet$ radical has a doublet ground state, there are only two possible states for the radical–radical pairs selected in step 1: singlet and triplet states. The value of J_{AB} for each pair is obtained from the energy difference between the lowest open-shell singlet and triplet states with the broken-symmetry approach^[40] used to describe the open-shell singlet state. Within this approximation the value of J_{AB} for the Hamiltonian described in [Eq. (2)] is obtained as $2J_{AB} = 2(E_{\text{BS}}^{\text{S}} - E^{\text{T}})$, in which E^{T} and E_{BS}^{S} are the energies of the triplet and broken-symmetry singlet states, respectively. Our experience indicates that $J_{AB} = (E_{\text{BS}}^{\text{S}} - E^{\text{T}})$ gives results that are closer to the experimental values than alternative ones in which projection is used.^[26–32, 41] Note that there has been some controversy about the use of projection when computing the values of the J_{AB} parameters by using the broken-symmetry approach within the DFT context (for detailed discussions, see reference [42]). Each of the J_{AB} values were separately calculated for the 160 and 12 K crystal structures by using the crystal geometry that each radical pair adopts. Energies were computed at the DFT/UB3LYP level^[43] with a 6–31 + G(d) basis set^[44] by using the Gaussian suite of programs.^[45] This level of theory has been previously shown to be appropriate for thiazyl derivatives.^[46]

$$\hat{H} = -2 \sum_{A,B} J_{AB} \hat{S}_A \cdot \hat{S}_B \quad (2)$$

Step 3) Determination of the magnetic topology of the crystal and its minimal magnetic model space: The magnetic topology is defined as the network of connections that the non-negligible J_{AB} magnetic interactions establish among the radicals (we have previously estimated that all interactions with $|J_{AB}| > 0.05 \text{ cm}^{-1}$ can be considered as significant). From the magnetic topology, the smallest finite model of radicals in which all non-negligible J_{AB} interactions are present in a ratio as similar as possible to that in the original infinite crystal can be defined, hereafter called the minimal magnetic model. This model allows the computation of the macroscopic magnetic properties from the values of the J_{AB} interactions by using statistical mechanics. Note that the extension of the minimal magnetic model space along the three crystallographic axes must clearly reproduce the magnetic topology of the infinite crystal. Furthermore, as the magnetic model space is enlarged, the computed macroscopic magnetic properties must converge towards the experimental result.

Step 4) Calculation of the macroscopic magnetic properties of the crystal by using the appropriate statistical mechanics expressions: Once the J_{AB} values have been computed in step 2, the matrix representation of the Heisenberg Hamiltonian given in [Eq. (2)] can be computed and diagonalized. Such a representation is computed on the basis of spin eigenfunctions of the minimal magnetic model space. In our calculations, the equivalent form of the Heisenberg Hamiltonian given in [Eq. (3)] is used,

in which \hat{I}_{AB} is the identity operator and \hat{S}_A and \hat{S}_B are the spin operators acting on radicals A and B. Note that the energy spectrum computed by using either Hamiltonians in [Eq. (2)] or [Eq. (3)] results in the same energy differences between the eigenvalues. By using these eigenvalues, the macroscopic magnetic properties are computed by using appropriate statistical mechanics expressions. Note that the size of the matrix representation of the Heisenberg Hamiltonian increases with the number of doublet radical N centers as $N!/[(N/2)!(N/2)!]$. Currently, we can fully diagonalize up to 16 different doublet centers. It is important to note that the magnetic field is included in the derivation of $\chi(T)$, although in most calculations and experimental work it is taken as negligible (zero magnetic field limit). In our procedure, for simplicity, the magnetic field is taken to be parallel to the easy axis of alignment $g\mu_B H \hat{S}_z$ (if any). Thus, it results in the value of χ parallel to the easy axis.

$$\hat{H} = -2 \sum_{A,B} J_{AB} \left(\hat{S}_A \cdot \hat{S}_B + \frac{1}{4} \hat{I}_{AB} \right) \quad (3)$$

This first-principles *bottom-up* approach^[26] enables the macroscopic properties (e.g., magnetic susceptibility and heat capacity) to be connected with their microscopic origin, that is, the J_{AB} exchange interactions. Consequently, it provides a rational analysis of the magnetic properties of a crystal and has provided excellent agreement with observation.^[27–32] Note that some theoretical studies have utilized steps 1 and 2 to evaluate J_{AB} but did not compute the macroscopic magnetic properties.^[47–53] Conversely, a likely exchange pathway and magnetic topology can be ‘guessed’ and a parametric Heisenberg spin Hamiltonian (only step 4) can be utilized to extract estimated fitting J parameters from experimental data.^[54–66] The first-principles *bottom-up* procedure^[26] described above combines these two approaches. The correct exchange pathway(s) and magnetic topology are determined at the microscopic level through the determination of possible J_{AB} values. Full matrix diagonalization of an appropriate magnetic model allows a direct comparison of calculated and experimental macroscopic magnetic properties, connecting their shape with the microscopic J_{AB} radical–radical interactions.

Results and Discussion

Comparative analysis of the crystal structures at 160 and 12 K: To compare the magnetic properties of $\beta\text{-}p\text{-NCC}_6\text{F}_4\text{CNSSN}^\bullet$ above and below the transition temperature (36 K), the pair-wise magnetic interactions were characterized by using crystal structures determined above (160 K) and below (12 K) the magnetic ordering temperature (see Table 2). The X-ray structure determined at 160 K has been previously reported,^[13a] whereas the structure determined at 12 K is reported herein (see Table 1, CCDC-755508). These single-crystal X-ray diffraction studies are in agreement with previous powder neutron diffraction studies^[14] and reveal that there is no structural phase transition associated with the magnetic transition at 36 K.

Throughout the temperature region studied, $\beta\text{-}p\text{-NCC}_6\text{F}_4\text{CNSSN}^\bullet$ adopts the noncentrosymmetric, orthorhombic space group $Fdd2$ with the molecule located on a two-fold axis and a total of eight radicals per unit cell (see Figure 1a for the 160 K structure). Although there is an expected contraction in the unit-cell volume upon cooling, the contraction along the crystallographic c axis (0.07%) is substantially smaller than the contraction along either the a or the b axes (1.25 and 0.85%, respectively). The rigidity of the c axis can be associated with the presence of short $\text{CN}^\delta-\cdots\text{S}^{\delta+}$ contacts (see Figure 1b), which generate a chain

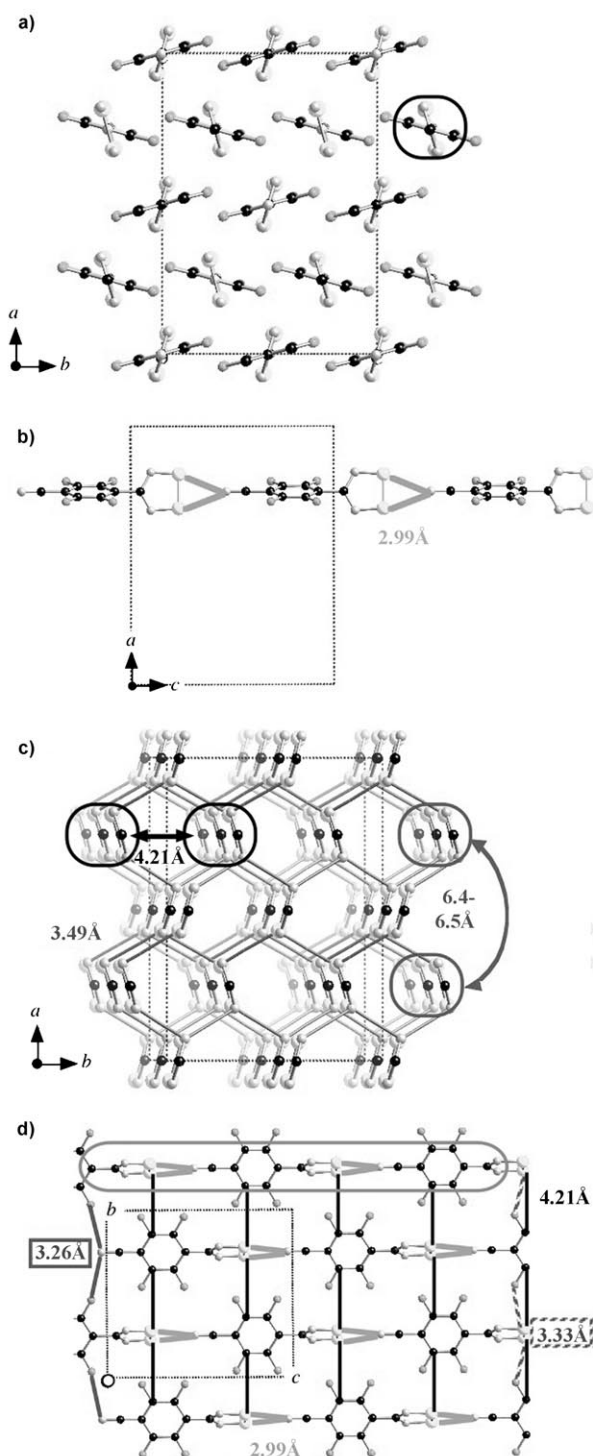


Figure 1. a) The unit cell ($Z=8$). b) View of encircled radical in (a) along the c axis forming chains. c) The ab view showing four symmetry-equivalent $S\cdots N$ closest contacts between heterocyclic rings (C_6F_4CN groups are omitted for clarity). Two next-nearest-neighbor sets of longer contacts are also schematically indicated, the closest of which are the $C\cdots S$ and $C\cdots N$ contacts. d) The bc view (encircled) of chain shown in (b) illustrating the slipped nature of adjacent chains along the c axis. Short $F\cdots NC$ and $F\cdots S$ interchain contacts are formed at 3.255(2) Å and 3.325(2) Å, respectively. Note that all distances apply to the 160 K crystal structure (see the main text for distances referring to the 12 K crystal structure).

motif parallel to this c axis. These offer both favorable electrostatic and dipolar contributions to the lattice enthalpy. These intermolecular contacts (2.986(3) Å at 160 K and 2.968(3) Å at 12 K) are considerably shorter than the sum of the van der Waals radii (3.35 Å)^[67] and present only a small variation in contacts upon cooling (see Table 3).

Table 2. Cell dimensions for the 160 and 12 K structures of the β - p -NCC $_6$ F $_4$ CN SSN' crystal (both belong to the $Fdd2$ space group). The difference between the crystallographic parameters is also given in the third row.

	a [Å]	b [Å]	c [Å]
12 K	14.913(3)	10.735(2)	11.925(2)
160 K	15.105(3)	10.828(2)	11.933(3)
contraction	0.192	0.093	0.008

The majority of the contraction of the unit-cell volume is accommodated by significant changes to the crystallographic a and b parameters, which lead to marked changes in the interchain interactions. Each radical makes four crystallographically equivalent short $S^{\delta+}\cdots N^{\delta-}$ contacts with radicals in nearby chains (see ab view in Figure 1c; $d_{S\cdots N}$ is 3.488(3) and 3.431(2) Å at 160 K and 12 K, respectively). In addition, the unit-cell contraction upon cooling leads to a shortening of the intermolecular contacts between the dithiadiazolyl ring and the C_6F_4 ring of a neighboring chain; the closest of these contacts is $C\cdots S$ (4.206(2) Å at 160 K, 4.172(2) Å at 12 K; see Figure 1c–d for a view in the ab and bc planes). Amongst the intermolecular distances between next-nearest neighbors, the shortest are $C\cdots S$ and $C\cdots N$ distances at approximately 6.4 and 6.5 Å, respectively (6.394(3) and 6.449(3) Å at 160 K, 6.295(2) and 6.407(2) Å at 12 K; see Figure 1c).

First-principles bottom-up study of β - p -NCC $_6$ F $_4$ CN SSN' by using 160 K and 12 K data: EPR and magnetic studies on the related PHTP- p -NCC $_6$ H $_4$ CN SSN' inclusion complex (PHTP=perhydrotriphenylene)^[68] indicated that there is no significant magnetic exchange through the structure-directing intrachain $CN\cdots S$ contacts (shown in Figure 1b). As a consequence, interactions through the interchain $S\cdots N$ contacts (shown in Figure 1c) were proposed according to the McConnell-I model as the only exchange pathway, generating a three-dimensional diamond-like exchange network^[68,17] with the small spontaneous moment arising through spin canting, which is allowed in the noncentrosymmetric space group $Fdd2$. This was supported by previous theoretical calculations on the 160 K structure.^[17]

Within the framework of our first-principles theoretical bottom-up procedure,^[26] all possible pairs of dithiadiazolyl radicals that might magnetically interact were identified. By using a 13.00 Å cut-off point between C atoms of the CN SSN rings, there are a total of 24 intermolecular contacts per radical. This cut-off includes all nearest-neighbor interactions, which are the usual candidates to exhibit strong exchange coupling. Because of the crystal symmetry, this re-

Table 3. Shortest intermolecular distances [\AA] for all eight radical pairs at 160 and 12 K selected in Step 1. The number of contacts per radical is also given.

radical pair di	No. of pairs per radical	160 K		12 K	
		$d[(\text{CNSSN}) \cdots (\text{CNSSN})]$	$d[(\text{CNSSN}) \cdots (\text{CNSSN})]$	$d[(\text{CNSSN}) \cdots (\text{CNSSN})]$	$d[(\text{CNSSN}) \cdots (\text{CNSSN})]$
$d1$	4	5.522(3)	3.488(3) (S \cdots N)	3.228(4) (N \cdots C)	5.476(2)
$d2$	2	9.293(1)	7.126(4) (N \cdots N)	6.822(3) (N \cdots F)	9.187(1)
$d3$	4	8.057(4)	6.419(2) (C \cdots S)	3.325(2) (S \cdots F)	8.023(3)
$d4$	4	9.625(3)	6.969(3) (S \cdots N)	6.394(3) (S \cdots C)	9.547(1)
$d5$	2	9.293(1)	8.062(4) (N \cdots N)	8.140(4) (N \cdots F)	9.187(1)
$d6$	4	9.440(2)	8.343(3) (S \cdots N)	6.537(2) (S \cdots F)	9.360(2)
$d7$	2	10.828(2)	10.828(2) ^[a]	8.678(3) (N \cdots F)	10.735(2)
$d8$	2	11.933(3)	9.734(4) (C \cdots S)	2.986(3) (S \cdots N)	11.925(2)

[a] CNSSN rings are related through translation parallel to the b axis, so all contacts between equivalent atoms are 10.828(2) \AA . (see the Supporting Information Table S1 for calculated singlet and triplet energies of the various dimer combinations at the two temperatures studied).

duces to just eight unique radical pairs (di , $i=1-8$). Table 3 lists the C \cdots C distance, the shortest contact between CNSSN rings, and the shortest intermolecular distance between CNSSN and C₆F₄CN rings for each radical pair at both 12 and 160 K (see Figure 2 and Table 3). A comparison of

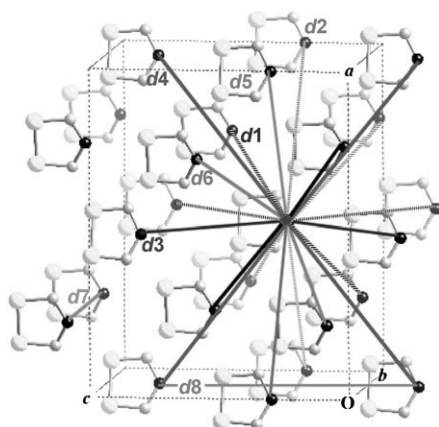


Figure 2. Eight radical pairs di , $i=1-8$, which exhibit heterocyclic contacts shorter than 13.00 \AA . Solid and shaded lines distinguish between contacts with front and rear molecules, respectively, for the same radical pair. For clarity, only the five-membered ring is shown for each radical.

Figure 1 and 2 clearly indicates that i) the short intrachain CN \cdots S distance at 2.986(3) \AA (in Figure 1b and d) corresponds to $d8$ (in Figure 2), ii) the interchain S \cdots N at 3.488(3) \AA (in Figure 1c) corresponds to $d1$ (in Figure 2), iii) S \cdots C at 4.206(2) \AA , S \cdots F at 3.325(2) \AA , and F \cdots NC at 3.255(2) \AA (in Figure 1c and d) correspond to $d3$ (in Figure 2), iv) C \cdots S at 6.394(3) \AA and C \cdots N at 6.449(3) \AA (in Figure 1c) correspond to $d4$ (in Figure 2). All contacts refer to the structure determined at 160 K.

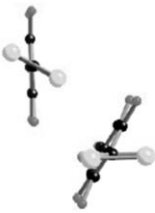
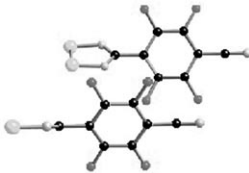
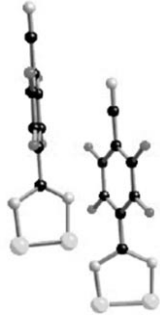

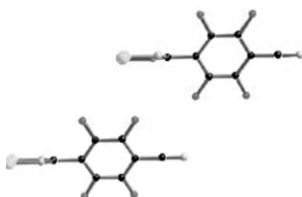
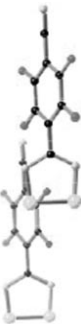

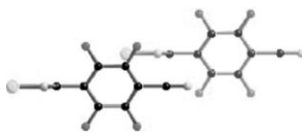
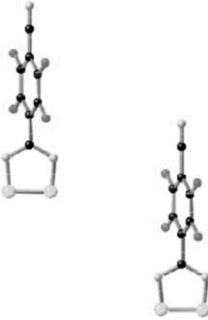
For each of the eight unique radical pairs ($d1-d8$), the microscopic $J(di)$ magnetic interactions were calculated at the UB3LYP/6-31+G(d) level.^[43,44] Calculations with the larger 6-311+G(d,p)^[69] basis set have been performed showing no appreciable variation in J values with results using 6-31+G(d)^[44] basis set (see the Supporting Information Table S2). At 160 K, DFT calculations indicate that the only non-negli-

gible magnetic interaction is $d1$, which exhibits a significant antiferromagnetic value ($J(d1)=-33.82 \text{ cm}^{-1}$). Calculation of the exchange interactions at 12 K resulted in an enhancement of the magnitude of the $J(d1)$ antiferromagnetic interaction from -33.82 cm^{-1} to -43.21 cm^{-1} and the appearance of two smaller ferromagnetic interactions $J(d3)=+7.64 \text{ cm}^{-1}$ and $J(d4)=+7.26 \text{ cm}^{-1}$ (see Table 4 for geometries). The strength of these ferromagnetic interactions has increased by over two orders of magnitude compared with their 160 K values, a fact that cannot be explained in terms of the variation of a single geometrical parameter. Note also that the geometry of these two contacts does not bring any regions of significant spin density (either positive or negative) into close proximity, which is contrary to the predictions of the McConnell-I model.^[23] Model calculations with the $p\text{-NCC}_6\text{F}_4$ groups replaced by H atoms (keeping the rest of the radicals fixed at their crystal-structure positions) show no sizable magnetic exchange coupling and we deduce that the perfluoroaryl group clearly plays an important role in propagating these ferromagnetic interactions.

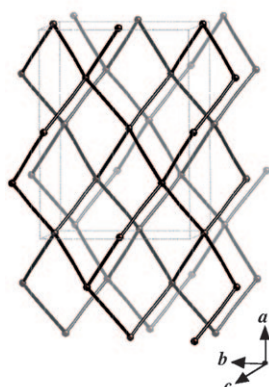
In the 160 K crystal structure, the magnetic topology generated by the only non-negligible J_{AB} pair interaction ($J(d1)=-33.82 \text{ cm}^{-1}$) is a three-dimensional diamond-like antiferromagnetic topology (see Figure 3a). Both the J_{AB} pair value and magnetic topology are in very good agreement with that estimated from the mean-field approach to the Curie-Weiss law^[13a] from [Eq. (1)] ($J/k=-34 \text{ cm}^{-1}$) by assuming a diamond-like exchange network ($z=4$).

In contrast, the exchange couplings computed by using the 12 K structure lead to a significantly more complex magnetic topology (Figure 3b) due to the simultaneous presence of ferro- (FM) and antiferromagnetic (AFM) J_{AB} interactions. Whereas the $J(d1)$ interactions maintain the 3D AFM diamond-like magnetic topology (Figure 3b, black), the FM $J(d3)$ (Figure 3b, blue) and $J(d4)$ (Figure 3b, red) interactions propagate in the bc and ac planes, respectively. Interestingly, the magnetic topology created by $J(d3)$ and $J(d4)$ FM interactions presents two independent interpenetrating ferromagnetic sublattices, which are antiferromagnetically coupled through the $J(d1)$ interaction (see the inset in Figure 3b for a better realization). Figure 4 illustrates the spin arrangement to visualize the essential antiferromagnetic

Table 4. General common rearrangement of $d1$, $d3$, and $d4$ radical pairs. The shortest radical–radical distances are given in Table 3. See the Supporting Information Table S3 for Mulliken's spin population of CNSSN rings.

d_i	T [K]	$J(d_i)$ [cm^{-1}]	ab view	bc view	ac view
$d1$	160	−33.82			
	12	−43.21			
$d3$	160	−0.02			
	12	+7.64			
$d4$	160	+0.02			
	12	+7.26			

a) $J(d1) = -33.82 \text{ cm}^{-1}$



b) $J(d1) = -43.21 \text{ cm}^{-1}$

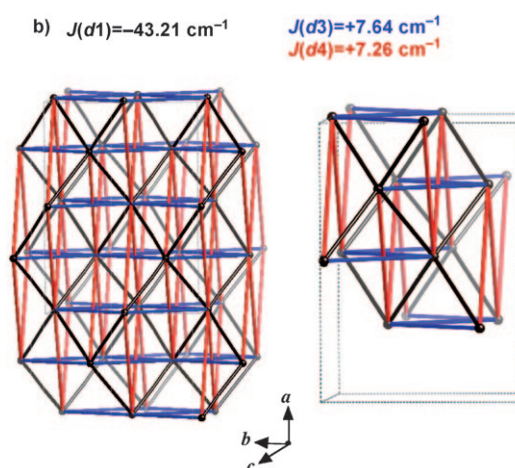


Figure 3. Three-dimensional magnetic topology drawn for the crystallographic unit cell. a) Diamond-like anti-ferromagnetic exchange topology based on the 160 K structural data; b) at 12 K, the topology can be seen as two interpenetrating ferromagnetic sublattices (red and blue networks, see inset) interconnected by anti-ferromagnetic interactions (black).

alignment depicting just one of the spin moments belonging to FM sublattice I (in orange), which is antiferromagnetically coupled to four nearest-neighbor spins belonging to FM sublattice II (in green) following a diamond-like arrangement. In addition, this same spin moment is ferromagnetically coupled to eight spins within the same sublattice I: four radicals through $J(d3)$ and another four radicals through $J(d4)$ along the bc and ac planes, respectively. Each center thus establishes four AFM and eight FM exchange interactions. This topology can be viewed as an extension of the usual textbook

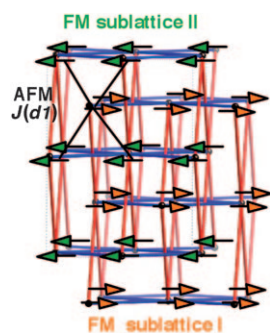


Figure 4. Qualitative representation to visualize the essential antiferromagnetic alignment of β - p -NCC₆F₄CN₂SSN' magnet (the easy axis of alignment is parallel to the b axis; the crystallographic axes are as in Figure 3), distinguishing between FM sublattices I and II by colored arrows (orange and green, respectively). The AFM interconnection between these sublattices (in black) is only shown in the upper-left corner.

explanation on the existence of spin canting (or weak ferromagnetism), which could be produced as a consequence of any small anisotropic preference in the interaction between the two antiparallel FM networks (no frustration is required).^[70] The isotropic nature of the calculated J_{AB} interactions from [Eq. (2)] and [Eq. (3)] does not provide any indication of the preferred spin orientation (easy axis) in the magnetically ordered phase. However, by using only an isotropic Heisenberg Hamiltonian, we can predict a topology that allows the existence of canting in the system, as in this case (Figure 4). The anisotropy associated with the presence of an antisymmetric exchange (Dzyaloshinsky–Moriya) term can induce a torque on each unpaired electron, which can in turn generate

a net spin moment, that is, the compound can exhibit canted antiferromagnetism. The value of the canting angle has been estimated to be as small as $0.14(3)$ – $0.26(2)^\circ$ from EPR and magnetization measurements.^[14]

In this magnetically ordered regime there are both field-dependent and field-independent contributions to the sample magnetization such that at any given temperature below the Neel temperature (T_N) [Eq. (4)] must hold true.

$$M(H,T) = \chi(T)H + M_s \quad (4)$$

The first term is equivalent to the residual magnetic susceptibility expected for a pure antiferromagnet without a spontaneous moment, whereas the second term arises from the spontaneous magnetic moment associated with spin canting. The spontaneous moment associated with spin canting leads to an abrupt discontinuity in $\chi(T)$ at the magnetic ordering temperature, which masks more subtle changes in the magnetic topology. However the isothermal field dependence of the magnetization $M(H,T)$ allows the determination of M_s and residual $\chi(T)$ directly at each temperature.^[13a] Figure 5 illustrates $\chi(T)$ in the paramagnetic regime (Figure 5, ●) and below T_N after subtracting the spontaneous contribution, M_s , to the sample magnetization (Figure 5, ○).

The minimal magnetic models that describe the 12 K (twelve-radical-center model, see Figure 6a) and 160 K (six-radical-center model, see Figure 6b) structures of the β - p -NCC₆F₄CN₂SSN' crystal were used to compute the magnetic susceptibility curve, $\chi(T)$. The $\chi(T)$ curve that was computed by using the minimal magnetic model for the 160 K crystal structure provides an excellent fit over the entire paramag-

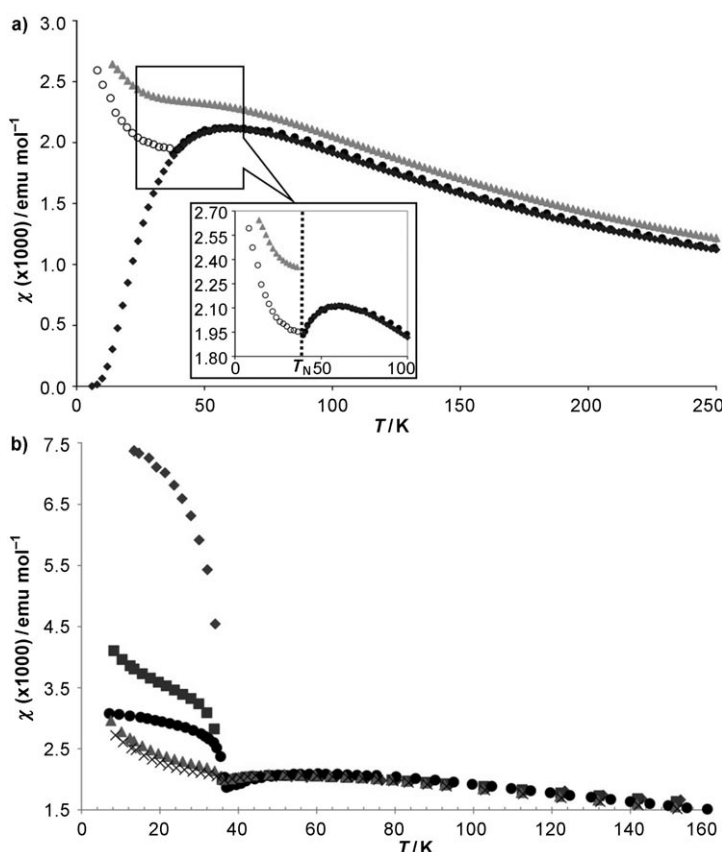


Figure 5. a) A $\chi(T)$ plot showing a comparison between experimental data above 36 K (●, measured in a field of 1 T) and extrapolated from $M(H,T)$ data below 36 K (○) and the simulation carried out by using minimal magnetic models of crystal structures of β - p -NCC₆F₄CN₂SSN' determined at 12 K (▲, corresponding to Figure 6a) and 160 K (◆, corresponding to Figure 6b). b) Raw $\chi(T)$ data at different magnetic fields (there is no subtraction of M_s ; ◆ = 0.1 T, ■ = 0.5 T, ● = 1 T, ▲ = 3 T, × = 5 T).

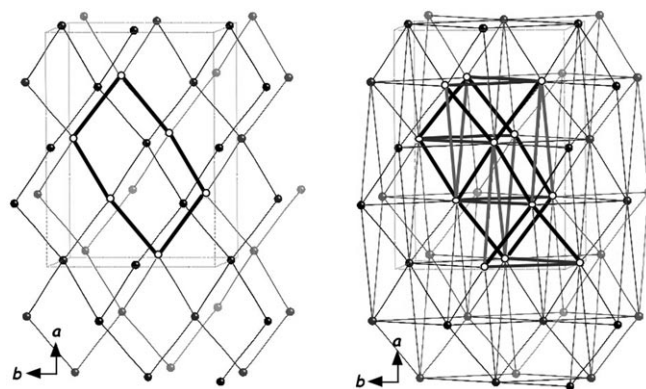


Figure 6. Minimal magnetic models inside the crystal itself at 160 K (left) and 12 K (right). Note that both minimal models are shown inside its corresponding magnetic topology.

netic region, from 36–300 K (see Figure 5). In particular it accurately reproduces both the position and height of the broad maximum of the experimental $\chi(T)$. Below 36 K, by

using the 160 K magnetic model, the computed $\chi(T)$ curve behaves in an analogous manner to the parallel (easy-axis) component of $\chi(T)$ of a typical antiferromagnet, with an exponential decay towards zero as T decreases. Experimentally, we observe a local minimum in $\chi(T)$ below 36 K, indicating a deficiency in the high-temperature model. Conversely, the computed data based on the 12 K magnetic model reflects the observed upturn in $\chi(T)$ upon cooling, supporting the thermal evolution of additional ferromagnetic exchange interactions within the magnetic lattice. This has also been recently observed in other studies.^[71]

Conclusion

The sudden variation of the magnetism of the β - p -NCC₆F₄CN₂SSN' crystal at 36 K is experimentally known to arise through spin canting. However, a detailed analysis of the magnetic susceptibility $\chi(T)$, having subtracted the dominant contribution arising from spin canting, reveals a turning point in the residual susceptibility below T_N . This change in $\chi(T)$ has been analyzed by performing a first-principles *bottom-up* study by using crystal data above (160 K) and below (12 K) the magnetic transition temperature. The procedure is a first-principles procedure because the magnetic exchange J_{AB} interaction for each radical pair is computed by using DFT methods. The procedure is also *bottom-up* because the macroscopic magnetic properties are obtained from the microscopic J_{AB} radical–radical magnetic interactions. This theoretical study indicates a change in the values of the microscopic J_{AB} exchange terms caused by the anisotropy of the thermal expansion. Whereas only one J_{AB} radical–radical pair is magnetically relevant ($J(d1) = -33.82 \text{ cm}^{-1}$) at 160 K, there are three significant radical–radical pairs based on the 12 K structure ($J(d1) = -43.21$, $J(d3) = +7.64$ and $J(d4) = +7.26 \text{ cm}^{-1}$). The magnetic topologies of the 160 and 12 K structures, therefore, differ: the 160 K structure presents a 3D diamond-like topology, whereas the topology of the 12 K structure is formed by two interpenetrating ferromagnetic sublattices that are antiferromagnetically coupled by $J(d1)$. This change in the magnetic topology gives rise to two different computed magnetic susceptibility curves. Whereas the high-temperature model predicts a decrease in the residual value of χ below T_N , the low-temperature model reproduces the observed increase in χ upon cooling below 36 K. The structural studies reveal the presence of significant anisotropy in the thermal expansion of the crystal, which leads to marked changes in the nature of the intermolecular magnetic exchange interactions. This emphasizes the importance of using crystal structure data measured at similar temperatures to the studied magnetic properties.

Acknowledgements

The authors thank the Spanish Science and Education Ministry for support (projects BQU2002-04587-C02-02, CTQ2005-02329 and, UNBA05-33-001), the Catalan DURSI (grants 2005SGR-00036 and 2005PEIR-0051/69), and the computer time allocated by CIESCA and BSC. M.D. thanks the Spanish Science and Education Ministry for the award of a ‘‘Ram3n y Cajal’’ Fellowship. This project was partly supported by EPSRC (UK) under grant GR/M86750 (ROPA) and the European Community under project HPRI-1999-CT-00071 by ‘Access to Research Infrastructure action’ of the Improving Human Potential Programme.

- [1] W. Heisenberg, *Z. Phys.* **1928**, *49*, 619.
- [2] M. Tamura, Y. Nakazawa, D. Shiomi, K. Nozawa, Y. Hosokoshi, M. Ishikawa, M. Takahashi, M. Kinoshita, *Chem. Phys. Lett.* **1991**, *186*, 401.
- [3] S. Nakatsuji, H. Anzai, *J. Mater. Chem.* **1997**, *7*, 2161.
- [4] M. P. Allemand, K. C. Khemani, A. Koch, F. Wudl, K. Holczer, S. Donovan, G. Gruner, J. D. Thompson, *Science* **1991**, *253*, 301.
- [5] R. Chiarelli, M. A. Novak, A. Rassat, J. L. Tholence, *Nature* **1993**, *363*, 147.
- [6] M. Mito, H. Nakano, T. Kawae, M. Hitaka, S. Takagi, H. Deguchi, K. Suzuki, K. Mukai, K. Takeda, *J. Phys. Soc. Jpn.* **1997**, *66*, 2147.
- [7] A. Alberola, J. M. Rawson, A. Whalley, *J. Mater. Chem.* **2006**, *16*, 2560.
- [8] W. Fujita, K. Awaga, *Chem. Phys. Lett.* **2002**, *357*, 385.
- [9] W. Fujita, K. Awaga, Y. Nakazawa, K. Saito, M. Sorai, *Chem. Phys. Lett.* **2002**, *352*, 348.
- [10] a) C. M. Robertson, D. J. T. Myles, A. A. Leitch, R. W. Reed, B. M. Dooley, N. L. Frank, P. A. Dube, L. K. Thompson, R. T. Oakley, *J. Am. Chem. Soc.* **2007**, *129*, 12688; b) C. M. Robertson, A. A. Leitch, K. Cvrkalj, R. W. Reed, D. J. T. Myles, P. A. Dube, R. T. Oakley, *J. Am. Chem. Soc.* **2008**, *130*, 8414.
- [11] a) A. A. Leitch, J. L. Brusso, K. Cvrkalj, R. W. Reed, C. M. Robertson, P. A. Dube, R. T. Oakley, *Chem. Commun.* **2007**, 3368; b) A. A. Leitch, X. Yu, S. M. Winter, R. A. Secco, P. A. Dube, R. T. Oakley, *J. Am. Chem. Soc.* **2009**, *131*, 7112.
- [12] A. Alberola, R. J. Less, C. M. Pask, J. M. Rawson, F. Palacio, P. Ollite, C. Paulsen, A. Yamaguchi, R. D. Farley, D. M. Murphy, *Angew. Chem.* **2003**, *115*, 4930; *Angew. Chem. Int. Ed.* **2003**, *42*, 4782.
- [13] A. J. Banister, N. Bricklebank, I. Lavender, J. M. Rawson, C. I. Gregory, B. K. Tanner, W. Clegg, M. R. J. Elsegood, F. Palacio, *Angew. Chem.* **1996**, *108*, 2648; *Angew. Chem. Int. Ed. Engl.* **1996**, *35*, 2533.
- [14] F. Palacio, G. Antorrena, M. Castro, R. Burriel, J. M. Rawson, J. N. B. Smith, N. Bricklebank, J. J. Novoa, C. Ritter, *Phys. Rev. Lett.* **1997**, *79*, 2336.
- [15] F. L. Pratt, A. E. Goeta, F. Palacio, J. M. Rawson, J. N. B. Smith, *Physica B: Condensed Matter* **2000**, *289*, 119.
- [16] P. J. Alonso, G. Antorrena, J. I. Mart3nez, J. J. Novoa, F. Palacio, J. M. Rawson, J. N. B. Smith, *Appl. Magn. Reson.* **2001**, *20*, 231.
- [17] a) J. Luz3n, J. Campo, F. Palacio, G. J. McIntyre, J. M. Rawson, *Polyhedron* **2005**, *24*, 2579; b) J. M. Rawson, J. Luz3n, F. Palacio, *Coord. Chem. Rev.* **2005**, *249*, 2631.
- [18] M. Mito, T. Kawae, K. Takeda, S. Takagi, Y. Matsushita, H. Deguchi, J. M. Rawson, F. Palacio, *Polyhedron* **2001**, *20*, 1509.
- [19] S. Blundell, *Magnetism in Condensed Matter*, Oxford University Press Inc., New York, **2001**.
- [20] A. Alberola, C. M. Pask, J. M. Rawson, E. J. L. McInnes, J. Wolowska, H. El-Kmani, G. M. Smith, *J. Phys. Chem. B* **2003**, *107*, 14158.
- [21] *Molecular Magnetism: New Magnetic Materials*, (Eds.: K. Itoh, M. Kinoshita), Gordon and Breach, Kodansha, **2000**.
- [22] *Magnetic Properties of Organic Materials*, (Ed.: P. Lahti), Marcel-Dekker: New York, **1999**.
- [23] H. M. McConnell, *J. Chem. Phys.* **1963**, *39*, 1910.
- [24] M. Deumal, J. J. Novoa, M. J. Bearpark, P. Celani, M. Olivucci, M. A. Robb, *J. Phys. Chem. A* **1998**, *102*, 8404.

- [25] J. Veciana, J. Cirujeda, J. J. Novoa, M. Deumal in *Magnetic Properties of Organic Materials*, (Ed.: P. Lahti), Marcel-Dekker: New York, **1999**, Chapter 28.
- [26] M. Deumal, M. J. Bearpark, J. J. Novoa, M. A. Robb, *J. Phys. Chem. A* **2002**, *106*, 1299.
- [27] M. Deumal, M. J. Bearpark, M. A. Robb, Y. Pontillon, J. J. Novoa, *Chem. Eur. J.* **2004**, *10*, 6422.
- [28] M. Deumal, F. Mota, M. J. Bearpark, M. A. Robb, J. J. Novoa, *Mol. Phys.* **2006**, *104*, 857.
- [29] J. Jornet, M. Deumal, J. Ribas-Ariño, M. J. Bearpark, M. A. Robb, R. G. Hicks, J. J. Novoa, *Chem. Eur. J.* **2006**, *12*, 3995.
- [30] A. Shapiro, C. P. Landee, M. M. Turnbull, J. Jornet, M. Deumal, J. J. Novoa, M. A. Robb, *J. Am. Chem. Soc.* **2007**, *129*, 952.
- [31] L. Lixin, M. M. Turnbull, C. P. Landee, J. Jornet, M. Deumal, J. J. Novoa, J. L. Wikaira, *Inorg. Chem.* **2007**, *46*, 11254.
- [32] M. Deumal, G. Giorgi, M. A. Robb, M. M. Turnbull, C. P. Landee, J. J. Novoa, *Eur. J. Inorg. Chem.* **2005**, 4697.
- [33] R. C. B. Copley, A. E. Goeta, C. W. Lehmann, J. C. Cole, D. S. Yufit, J. A. K. Howard, J. M. Archer, *J. Appl. Crystallogr.* **1997**, *30*, 413.
- [34] J. R. Allibon, MAD diffractometer Control Software-AlphaVMS Version, Institut Laue-Langevin (DPT/SCI), Grenoble, France, **1996**.
- [35] a) M. S. Lehmann, S. Wilson, COLL5N. College V, *Data reduction system*, Institut Laue-Langevin, Grenoble, France, **1987**; b) M. S. Lehmann, F. K. Larsen, *Acta Crystallogr.* **1974**, *A30*, 580.
- [36] G. M. Sheldrick, *Acta Crystallogr.*, **1990**, *A46*, 467.
- [37] G. M. Sheldrick, SHELXL93, *Program for the Refinement of Crystal Structures*, University of Göttingen, Göttingen, Germany, **1997**.
- [38] J. Luzón, J. Campo, F. Palacio, G. J. McIntyre, A. E. Goeta, E. Res-souche, C. M. Pask, J. M. Rawson, *Physica B: Condensed Matter* **2003**, *335*, 1–5.
- [39] a) For verdazyl derivatives, see reference [28] (triradical model); for dithiazolyl derivatives, see: b) G. D. McManus, *J. Mater. Chem.* **2001**, *11*, 1992; c) W. Fujita, K. Awaga, *Science* **1999**, *286*, 261 (TTTA, tri-radical model); d) Cu(2,3-dmpz)Br₂ in *J. Mol. Cat. A: Chem.* **2005**, *228*, 117 (triradical and tetraradical models).
- [40] a) L. Noodleman, *J. Chem. Phys.* **1981**, *74*, 5737–5746; b) L. Noodleman, E. R. Davidson, *Chem. Phys.* **1986**, *109*, 131–143.
- [41] E. Ruiz, P. Alemany, S. Alvarez, J. Cano, *J. Am. Chem. Soc.* **1997**, *119*, 1297–1303.
- [42] a) E. Ruiz, S. Alvarez, J. Cano, V. Polo, *J. Chem. Phys.* **2005**, *123*, 164110/1–7; b) C. Adamo, V. Barone, A. Bencini, R. Broer, M. Filatov, N. M. Harrison, F. Illas, J. P. Malrieu, I. P. R. Moreira, *J. Chem. Phys.* **2006**, *124*, 107101/1–3.
- [43] a) A. D. Becke, *Phys. Rev. A* **1988**, *38*, 3098; b) A. D. Becke, *J. Chem. Phys.* **1993**, *98*, 5648; c) C. Lee, W. Yang, R. G. Parr, *Phys. Rev. B* **1988**, *37*, 785.
- [44] For the 6-31+G[d] split-valence basis set, see: a) P. C. Hariharan, J. A. Pople, *Theor. Chim. Acta* **1973**, *28*, 213; b) M. M. Francl, W. J. Pietro, W. J. Hehre, J. S. Binkley, M. S. Gordon, D. J. DeFrees, J. A. Pople, *J. Chem. Phys.* **1982**, *77*, 3654.
- [45] M. J. Frisch, G. W. Trucks, H. B. Schlegel, G. E. Scuseria, M. A. Robb, J. R. Cheeseman, V. G. Zakrzewski, J. A., Jr., Montgomery, R. E. Stratmann, J. C. Burant, S. Dapprich, J. M. Millam, A. D. Daniels, K. N. Kudin, M. C. Strain, O. Farkas, J. Tomasi, V. Barone, M. Cossi, R. Cammi, B. Mennucci, C. Pomelli, C. Adamo, S. Clifford, J. Ochterski, G. A. Petersson, P. Y. Ayala, Q. Cui, K. Morokuma, D. K. Malick, A. D. Rabuck, K. Raghavachari, J. B. Foresman, J. Cioslowski, J. V. Ortiz, A. G. Baboul, B. B. Stefanov, G. Liu, A. Liashenko, P. Piskorz, I. Komaromi, R. Gomperts, R. L. Martin, D. J. Fox, T. Keith, M. A. Al-Laham, C. Y. Peng, A. Nanayakkara, C. Gonzalez, M. Challacombe, P. M. W. Gill, B. Johnson, W. Chen, M. W. Wong, J. L. Andres, C. Gonzalez, M. Head-Gordon, E. S. Replogle, J. A. Pople, Gaussian 98, Revision A.7, Gaussian, Inc., Pittsburgh PA, **1998**.
- [46] a) M. Deumal, S. LeRoux, J. M. Rawson, M. A. Robb, J. J. Novoa, *Polyhedron* **2007**, *26*, 1949; b) J. Jornet, M. A. Robb, M. Deumal, J. J. Novoa, *Inorg. Chim. Acta* **2008**, *361*, 3586.
- [47] P. Wind, N. Guihéry, J. P. Malrieu, *Phys. Rev. B* **1999**, *59*, 2556.
- [48] I. P. R. Moreira, F. Illas, C. J. Calzado, J. F. Sanz, J. P. Malrieu, N. Ben Amor, D. Maynau, *Phys. Rev. B* **1999**, *59*, R6593.
- [49] M. Mitani, H. Mori, Y. Takano, D. Yamaki, Y. Yoshioka, K. Yamaguchi, *J. Chem. Phys.* **2000**, *113*, 4035.
- [50] C. Blanchet-Boiteux, J. M. Mouesca, *J. Phys. Chem. A* **2000**, *104*, 2091.
- [51] A. Rodriguez-Fortea, P. Alemany, S. Alvarez, E. Ruiz, *Chem. Eur. J.* **2001**, *7*, 627.
- [52] F. Illas, I. D. R. Moreira, C. de Graaf, V. Barone, *Theor. Chem. Acc.* **2000**, *104*, 265.
- [53] C. Kolczewski, K. Fink, V. Staemmler, *Int. J. Quantum Chem.* **2000**, *76*, 137.
- [54] G. A. Baker, G. S. Rushbrooke, H. E. Gilbert, *Phys. Rev. A* **1964**, *135*, 1272.
- [55] W. Duffy, K. P. Barr, *Phys. Rev.* **1968**, *165*, 647.
- [56] K. M. Diederix, H. W. J. Blöte, J. P. Groen, T. O. Klaassen, N. J. Poulis, *Phys. Rev. B* **1979**, *19*, 420.
- [57] J. W. Hall, W. E. Marsh, R. R. Weller, W. E. Hatfield, *Inorg. Chem.* **1981**, *20*, 1033.
- [58] W. E. Hatfield, *J. Appl. Phys.* **1981**, *52*, 1985.
- [59] E. Coronado, M. Drillon, A. Fuertes, D. Beltran, A. Mosset, J. Galy, *J. Am. Chem. Soc.* **1986**, *108*, 900.
- [60] T. Barnes, E. Dagotto, J. Riera, E. S. Swanson, *Phys. Rev. B* **1993**, *47*, 3196.
- [61] J. J. Borrás-Almenar, E. Coronado, J. Curely, R. Georges, J. C. Gians-duzzo, *Inorg. Chem.* **1994**, *33*, 5171.
- [62] T. Barnes, J. Riera, *Phys. Rev. B* **1994**, *50*, 6817.
- [63] J. J. Borrás-Almenar, J. M. Clemente-Juan, E. Coronado, F. Lloret, *Chem. Phys. Lett.* **1997**, *275*, 79.
- [64] T. Barnes, J. Riera, D. A. Tennant, *Phys. Rev. B* **1999**, *59*, 11384.
- [65] J. J. Borrás-Almenar, J. M. Clemente-Juan, E. Coronado, B. S. Tsu-kerblat, *Inorg. Chem.* **1999**, *38*, 6081.
- [66] J. J. Borrás-Almenar, J. M. Clemente-Juan, E. Coronado, B. S. Tsu-kerblat, *J. Comput. Chem.* **2001**, *22*, 985.
- [67] J. G. Stark, H. G. Wallace, *Chemistry Data Book; SI Edition*, John Murray, London, **1980**.
- [68] P. J. Langley, J. M. Rawson, J. N. B. Smith, M. Schuler, R. Bachmann, A. Schweiger, F. Palacio, G. Antorrena, G. Gescheidt, A. Quintel, P. Rechsteiner, J. Hulliger, *J. Mater. Chem.* **1999**, *9*, 1431.
- [69] For 6-311+G(d,p), see: a) R. Krishnan, J. S. Binkley, R. Seeger, J. A. Pople, *J. Chem. Phys.* **1980**, *72*, 650; b) A. D. McLean, G. S. Chandler, *J. Chem. Phys.* **1980**, *72*, 5639; c) T. Clark, J. Chandrasekhar, G. W. Spitznagel, P. v. R. Schleyer, *J. Comput. Chem.* **1983**, *4*, 294; d) M. J. Frisch, J. A. Pople, J. S. Binkley, *J. Chem. Phys.* **1984**, *80*, 3265.
- [70] R. L. Carlin, *Magnetochemistry*, Springer-Verlag, Berlin and Heidelberg **1986**, pp. 149–150.
- [71] a) S. M. Winter, K. Cvrkalj, P. A. Dube, C. M. Robertson, M. R. Probert, J. A. K. Howard, R. T. Oakley, *Chem. Commun.* **2009**, 7306; b) S. L. Veber, M. V. Fedin, A. I. Potapov, K. Yu. Maryunina, G. V. Romanenko, R. Z. Sagdeev, V. I. Ovcharenko, D. Goldfarb, E. G. Bagryanskaya, *J. Am. Chem. Soc.* **2008**, *130*, 2444–2445.

Received: November 25, 2009
Published online: February 5, 2010